

# Secular bar formation in galaxies with significant amount of dark matter

Octavio Valenzuela and Anatoly Klypin

*New Mexico State University, Las Cruces, NM 88001*

Accepted ...; Received ...; in original form ...

## ABSTRACT

Using high resolution N-body simulations of stellar disks embedded in cosmologically motivated dark matter halos, we study the evolution of bars and the transfer of angular momentum between halos and bars. We find that dynamical friction results in some transfer of angular momentum to the halo, but the effect is much smaller than previously found in low resolution simulations and is incompatible with early analytical estimates. After 5 Gyrs of evolution the stellar component loses only 5% – 7% of its initial angular momentum.

Mass and force resolutions are crucial for the modeling of bar dynamics. In low resolution (300 – 500 pc) simulations we find that the bar slows down and angular momentum is lost relatively fast. In simulations with millions of particles reaching a resolution of 20-40 pc, the pattern speed may not change over billions of years. Our high resolution models produce bars which are fast rotators, where the ratio of the corotation radius to the bar major semi-axis lies in the range  $\mathcal{R} = 1.2 - 1.7$ , marginally compatible with observational results. In contrast to many previous simulations, we find that bars are relatively short. As in many observed cases, the bar major semi-axis is close to the exponential length of the disk.

The transfer of angular momentum between inner and outer parts of the disk plays a very important role in the secular evolution of the disk and the bar. The bar formation increases the exponential length of the disk by a factor of 1.2 -1.5. The transfer substantially increases the stellar mass in the centre of the galaxy and decreases the dark matter-to-baryons ratio. As the result, the central 2 kpc region is always strongly dominated by the baryonic component. At intermediate (3 – 10 kpc) scales the disk is sub-dominant. These models demonstrate that the efficiency of angular momentum transfer to the dark matter has been greatly overestimated. More realistic models produce bar structure in striking agreement with observational results.

**Key words:** galaxies: kinematics and dynamics — galaxies: evolution.

## 1 INTRODUCTION

Making predictions for structure of individual galaxies in the framework of cosmological models is a difficult task, which until recently was mostly dominated by modeling of central parts dark matter dominated systems such as dwarf galaxies and low surface brightness galaxies (e.g., Moore 1994; Flores & Primack 1994; Kravtsov et al. 1998; van den Bosch & Swaters 2001; Lokas 2001; de Blok et al. 2001). It is generally accepted that models do not fare well on those tests predicting too fast rotation in the central region. Excessive amount of dark matter satellites is an additional complication for the cosmological models (Klypin et al. 1999; Moore et al. 1999).

Another layer of problems is on slightly larger scales: luminous parts of normal galaxies and masses in the range

of  $10^{10} - 10^{12} M_{\odot}$ . The number of issues is quite large. An excessive amount of the dark matter in the bulge may result in too few microlensing events (e.g., Zhao & Mao 1996; Binney & Evans 2001), but see also (Klypin et al. 2002). Mass modeling of the Milky Way galaxy on different scales is a complicated and quite uncertain issue (e.g., Dehnen & Binney 1998). For the halos predicted by cosmological models the conclusions change from very pessimistic (Navarro & Steinmetz 2000; Hernández et al. 2001) to neutral (Eke et al. 2001) to more optimistic (Klypin et al. 2002).

One of the contentious issues is the pattern speed of bars. Using analytical arguments and a combination of N-body simulations with rotating solid bars Weinberg (1985); Hernquist & Weinberg (1992) argued that a non-rotating dark matter will exert so much tidal friction that a bar should lose its angular momentum in few rotation periods.

For a rigid rotating bar with mass comparable to the mass of the spheroid (including possible dark matter) inside the bar radius Hernquist & Weinberg (1992) predict that the bar “sheds all its angular momentum typically in less than  $\sim 10^9$  yr”. If true, that would make impossible for bars to exist in galaxies with dark matter halos. There are no doubts that the dynamical friction operates when a bar rotates inside a dark matter halo. Yet, the rate and the amount of the angular momentum lost by the disk is still a matter of debate. Fully self-consistent N-body simulations with live bars, disks, and dark matter halos (Combes & Sanders 1981; Sellwood & Athanassoula 1986; Debattista & Sellwood 1998, 2000; Athanassoula & Misiriotis 2002) show that the bars slow down far less than what has been predicted by Weinberg (1985); Hernquist & Weinberg (1992). Bars in simulations rotate for billions of years, defying the theoretical expectations. Yet, the bars in numerical models are observed to slow down. Debattista & Sellwood (1998, 2000) find that in models, in which initially the dark matter constitutes about the same amount of mass as the stellar disk in the central part of the galaxy, the baryonic component (disk + bar) loses about 40 percent of its angular momentum over  $\sim 10$  Gyrs. The bar pattern speed declines by a factor of five after the bar forms. This produces a bar which rotates more than twice slower than the observed bars. The speed of bar rotation is often characterized by the ratio  $\mathcal{R}$  of radius of corotation to the large semi-axis of the bar. For few galaxies the ratio has been estimated  $\mathcal{R} = 1.1 - 1.7$  using stellar kinematics and the method of Tremaine & Weinberg (1984). Bars in models of Debattista & Sellwood (1998, 2000) have  $\mathcal{R} = 2.0 - 2.6$ , which contradicts the observed values.

A less known but not less important problem of the bars is their length. In most models (dark matter dominated or not) the semi-major axis of bars is 2-4 times longer than the exponential length of the disk (Debattista & Sellwood 1998, 2000; Athanassoula & Misiriotis 2002). This is significantly larger than for real galaxies, which typically have bar length of 0.5-1.5 of the exponential disk scale (Elmegreen & Elmegreen 1985). In our Galaxy the bar is 3-3.5 kpc long (Blitz & Spergel 1991; Zhao 1996; Freudenreich 1998; Gerhard 2002) which is close to the disk scale length of 2.5-3.5 kpc (Dehnen & Binney 1998; Hammersley et al. 1999; Gerhard 2002). In the case of the models studied by Debattista & Sellwood (1998, 2000) the bar extended over the whole disk. That would correspond to 15 kpc, if we scale the models to match our Galaxy. If we scale a dark matter dominated model MH of Athanassoula & Misiriotis (2002) to our Galaxy, the radius of the bar would be 14 kpc (about 4 exponential lengths), which seriously contradicts the observations.

The arguments – the slowing down of bars and the lengths of bars – against significant amount of the dark matter in the central parts of normal galaxies have problems on their own. The arguments are based on numerical simulations, which suffer from two types of problems: numerical effects and initial conditions. Numerical resolution is very limited in most simulations. It is often emphasized that models should have a large number of particles to suppress the two-body scattering and to reduce the noise (e.g., Weinberg 1998; Debattista & Sellwood 2000). Yet, the force resolution is another important effect. For example, the formal (one cell) resolution in simulations of Debattista & Sell-

wood (2000) was 1/5 of the disk scale length. If we scale the length to 3.5 kpc of our Galaxy, then we get the formal resolution of 700 pc. To make the things worse, the real resolution in a PM code is not the formal resolution. At distances close to the formal resolution the code is capable of producing and keeping density gradients of about 1.5 – 2. Only at about twice the formal resolution the force is close to the Newton’s law. For Debattista & Sellwood (1998) and Debattista & Sellwood (2000) simulations this corresponds to 1.4 kpc, which is clearly not enough to mimic the disk of our Galaxy. The resolution in simulations of Fux (1997) was 1.8 kpc at the solar distance.

Initial setup is questionable in many cases when it comes to the properties of the dark matter halo. If one wants to test predictions of cosmological models, those predictions should be used for setting initial conditions of numerical models. For example, halos predicted by cosmological models are very large and should extend to 200-300 kpc for galaxies of the size of our Galaxy (Klypin et al. 2002). Halos in simulations are much smaller than that. For example, Fux (1997) used halo truncated at 38 kpc. Models of Debattista & Sellwood (2000) were larger - 40 kpc, but still too small as compared to the virial radius of the halo of our Galaxy. The density profile in the outer part of a halo (radii larger 20 kpc for the Milky Way galaxy) should decline as  $\rho_{\text{dm}} \propto r^{-3}$  (Navarro et al. 1997). This is very different from the profiles used in many simulations of bar formation. For example, Fux (1997) used exponential profile  $\rho_{\text{DM}} \propto \exp(-r/9.1 \text{ kpc})$ . Athanassoula & Misiriotis (2002) used density profile  $\rho \propto \exp(-r^2/(35 \text{ kpc})^2)/[r^2 + (1.75 \text{ kpc})^2]$  truncated at 45 kpc. Debattista & Sellwood (2000) used polytropes  $n = 3$ , which have little relation with the expected dark matter profile.

Both problems of the existing numerical simulations – the resolution and the initial conditions – motivate us to simulate with high resolution models, which use more realistic initial conditions. We use the traditional approach to form a bar: bars are formed by dynamical instability in initially featureless equilibrium disk rotating inside halos (Hohl 1971; Ostriker & Peebles 1973; Miller 1978). In section 2 we describe initial conditions for our models and give details of the code used to run our simulations. The evolution of models is discussed in section 3. In section 4 we present results on the angular momentum of different components. The pattern speed and the structure of bars are presented in section 5. We discuss our results and compare them with the previous results in section 6. A brief summary of our conclusions is given in section 7

## 2 MODELS

### 2.1 Initial conditions: densities and velocities

We study models, which initially have only two components: an exponential disk and a dark matter halo. No initial bulge or a bar are used. Initial conditions for the systems are generated using Hernquist (1993) method. We use the following approximation for the density of the stellar disk in cylindrical coordinates:

$$\rho_d(R, z) = \frac{M_d}{4\pi z_0 R_d^2} e^{-\frac{R}{R_d}} \text{sech}^2(z/z_0), \quad (1)$$

where  $M_d$  is the mass of the disk,  $R_d$  is the exponential length, and  $z_0$  is the scale height. The later was assumed to be constant through the disk. The disk is truncated at five exponential lengths and at three scale heights:  $R < 5R_d$ ,  $z < 3z_0$ . Disk mass was slightly corrected to include the effects of truncation. The vertical velocity dispersion  $\sigma_z$  is related to the surface stellar density  $\Sigma$  and the disk height  $z_0$ :

$$\sigma_z^2(R) = \pi G z_0 \Sigma(R), \quad (2)$$

where  $G$  is the gravitational constant. The radial velocity dispersion  $\sigma_R$  is also assumed to be directly related to the surface density:

$$\sigma_R^2(R) = A e^{-\frac{R}{R_d}}. \quad (3)$$

The normalization constant  $A$  in eq. (3) is fixed in such a way that at some reference radius  $R_{\text{ref}}$  the radial random velocities are  $Q$  times the critical value needed to stabilize a differentially rotating disk against local perturbations:

$$\sigma_R(R_{\text{ref}}) = Q \frac{3.36 G \Sigma(R_{\text{ref}})}{\kappa(R_{\text{ref}})}, \quad (4)$$

where  $\kappa(R_{\text{ref}})$  is the epicycle frequency at the reference radius. The reference radius is chosen to be  $R_{\text{ref}} = 5$  kpc for our models. Results are very insensitive to the particular choice of the reference radius because the stability parameter  $Q$  does not change much for radii from  $R_d$  to few  $R_d$ . We also consider a family of models where  $Q$  is fixed along the disk. In this case eq.(4) gives the radial dispersion at every point. The fast increase of the epicycle frequency  $\kappa$  in the central region overcomes the exponential growth of density making the disk colder in the center.

The tangential ( $\phi$ ) component of the rotational velocity and its dispersion are found using the asymmetric drift and the epicyclic approximations:

$$V_\phi^2 = V_c^2 - \sigma_R^2 \left( \frac{2R}{R_d} + \frac{\kappa^2}{4\Omega^2} - 1 \right), \quad (5)$$

$$\sigma_\phi^2 = \sigma_R^2 \frac{\kappa^2}{4\Omega^2}. \quad (6)$$

Here the circular velocity  $V_c$  is found as the quadrature sum of the halo and the disk contributions. For the disk component we use the thin-disk approximation.

We assume that the dark matter density profile is described by the NFW profile (Navarro et al. 1997):

$$\rho_{\text{dm}}(r) = \frac{\rho_s}{x(1+x)^2}, \quad x = r/r_s, \quad (7)$$

$$M_{\text{vir}} = 4\pi\rho_s r^3 \left[ \ln(1+C) - \frac{C}{1+C} \right], \quad C = \frac{r_{\text{vir}}}{r_s}, \quad (8)$$

where  $M_{\text{vir}}$  and  $C$  are the virial mass and the concentration of the halo. For given virial mass the virial radius of the halo is found assuming a flat cosmological model with matter density parameter  $\Omega_0 = 0.3$  and the Hubble constant  $H_0 = 70 \text{ km s}^{-1} \text{ Mpc}^{-1}$ .

Knowing the mass distribution of the system  $M(r)$ , we find the radial velocity dispersion of the dark matter:

$$\sigma_{r,\text{dm}}^2 = \frac{1}{\rho_{\text{dm}}} \int_r^\infty \rho_{\text{dm}} \frac{GM(r)}{r^2} dr. \quad (9)$$

The other two components of the velocity dispersion are equal to  $\sigma_{r,\text{dm}}^2$ . In other words, the velocity distribution is

isotropic, which is a good approximation for the central parts of the dark matter halos (e.g., Colín et al. 2000). Eq.(9) ignores non-spherical deviations of the gravitational acceleration for the dark matter. At each radius we find the escape velocity and remove particles moving faster than the escape velocity.

The dark matter halo is truncated at the virial radius, which for our models is at 250 kpc – 300 kpc radius. During the evolution of the system, the truncation results in a gradual smearing of the outer boundary of the halo. Some particles move to radii larger than the virial radius. They are not replaced by other particles, which, in true equilibrium, would come from the region outside the truncation radius. This creates a rarefaction wave moving inside the halo. The wave never reached the central part of the halo and was always outside the central 100 kpc region.

The distributions eqs. (1-9) are used to produce initial coordinates and velocities of particles. The space is divided into bins. We estimate the expected number of particles inside each bin. We than randomly place specified number of particles inside the bin. Spherical shells are used to initiate the dark matter particles. For the disk we use cylindrical shells along radius and equal-spaced bins along the axis of rotation. Velocities are picked from an appropriate Gaussian distribution truncated at the escape velocity. The number of particles was typically 10-20 in each bin. The resulting distribution of particles was tested against expected analytical expressions.

The disks are realized with particles of an equal mass. The dark matter halo is composed of particles of variable mass with small particles placed in the central region and larger particles at larger distances. We double the particle mass as we move further and further from the center. In total we use 5 mass species with the mass range of 32. The region covered by small mass particles is  $\sim 40$  kpc – much larger than the size of the disk. In order to reduce the two-body scattering each dark matter particle in the central region has the same mass as a disk particle.

This procedure is designed to reduce the number of particles and, at the same time, to allow us to cover a very large volume. For example, in model  $A_1$  we have 3.55 million particles inside  $\sim 300$  kpc, of which 2.4 million are small particles. We would need 9.5 million particles, if particles of equal mass were used. In the course of evolution some of massive particles come closer to the center, but their number was always very small.

## 2.2 Choice of parameters

The approximation eq. (8) formally is valid only for pure dark matter halos without baryons. Contraction of baryons in the process of formation of the disk should significantly affect the dark matter. We try to mimic the effects of the contraction by changing the halo concentration and by tuning parameters of the halo and the disk in such a way that the distribution of the dark matter roughly approximates more realistic models. Klypin et al. (2002) presented such models for the Milky Way and for the M31 galaxies. The models used realistic cosmological dark matter halos and satisfied numerous observational constraints. To some degree we mimic two favored models in that paper: models  $A_1$  and  $B_1$ , which are described in detail in Klypin et al. (2002).

The first model ( $A_1$ ) was designed assuming that the angular momentum of the dark matter was preserved during baryonic collapse. The conservation of angular momentum leads to a specific prediction that in the central  $\sim 5$  kpc the density of the dark matter closely follows the density of the baryonic component. The second model ( $B_1$ ) includes effects of an exchange of angular momentum between the baryons and the dark matter. The dark matter gains angular momentum through the dynamical friction during early stages of disk and bulge formation, when non-axisymmetric perturbations are expected to be large. Somewhat similar scenario was proposed by El-Zant et al. (2001). Model  $B_1$  also had significant amount of the dark matter in the central region, but less than in model  $A_1$ . For example, the crossing point, at which the contribution of the dark matter to the circular velocity is equal to that of the baryons, is shifted from 5 kpc in model  $A_1$  to 12 kpc in model  $B_1$ .

In order to reproduce the effects of the contraction and the exchange of the angular momentum, we increase the concentration of the dark matter halos. Our models have  $C = 15$  as compared with  $C = 12$  for models of Klypin et al. (2002). We also adjust parameters of our models (virial mass, exponential length and mass of the disk) to roughly mimic important properties of Klypin et al. (2002) models in the central 20 kpc. For example, our models ( $A_1$  and  $A_2$ ) have a sub-maximum disk (contributions of the disk and the halo to the circular velocity are approximately equal) at radii  $R < 5$  kpc with halo dominating at larger radii. The mass of the disk was  $4.28 \times 10^{10} M_\odot$ , which is close to the mass of disk+bulge in model  $A_1$  of Klypin et al. (2002).

The only difference between our two models  $A_1$  and  $A_2$  is in the velocity dispersions of disk particles. For model  $A_1$  we use eq.(3) with the normalization provided by eq.(4) at the reference radius. In the case of model  $A_2$  the eq.(4) is used at all radii (not just at one radius) and the eq.(3) is not used at all. In other words, model  $A_2$  has the *same*  $Q$  parameter at all radii. The main difference between the models is that model  $A_2$  is “colder” in the central region. In the central  $\sim 1$  kpc region model  $A_2$  has significantly smaller radial and azimuthal velocity dispersions. Both models have the same circular velocity and the same vertical velocity dispersion.

Our next model ( $B$ ) has a smaller halo and a more massive disk ( $6 \times 10^{10} M_\odot$ ). The disk mass is equal to the sum of the disk and the bulge masses in model  $B_1$  of Klypin et al. (2002). Parameters of our models are presented in Table 1. Top panels in Figure 1 shows the initial circular velocities  $V_c = \sqrt{GM(r)/r}$  of the disk and the halo for the models.

There are important differences between our models and the models described in Klypin et al. (2002). The later are realistic models, which, in addition to the exponential disk and the halo, have also a nucleus and a triaxial bar. The goal of our paper is to study how a bar develops in an unstable disk. Thus, our models initially do not have either a bar or a bulge: all the stellar mass is in the exponential disk. The bar and the bulge are expected to form from the disk. Initially, our models to some degree mimic Klypin et al. (2002) models. For example, the exponential disk length is 3 – 3.5 kpc. Yet the subsequent evolution of the models was quite significant. Thus, the final parameters are rather different from what was assumed at the beginning. Our final models do not provide a fit to the Milky Way galaxy. Nevertheless, the

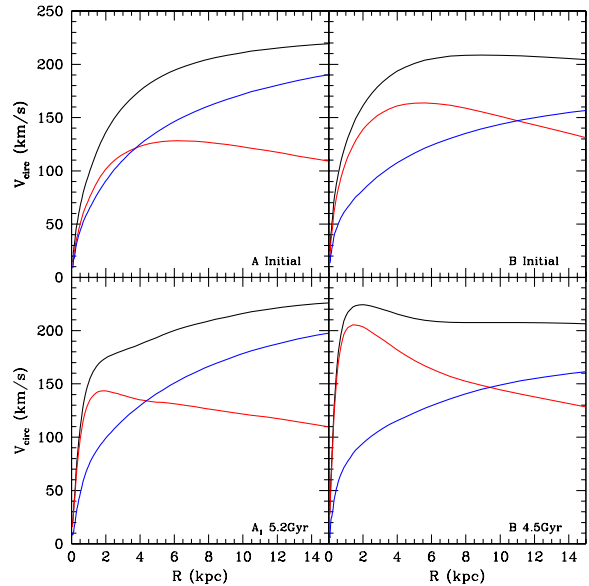


**Figure 1.** Initial and final circular velocities for model  $A_1$  (left panels) and for model  $B$  (right panels). Dashed curves show the contribution of the stellar component  $\sqrt{GM(r)/r}$ . The dot-dashed curves are for the dark matter. Final models show the total stellar contribution: disk and bar contributions are combined. Initially model  $A_1$  has a sub-maximum disk with the density of the disk being close to the density of the dark matter inside the central 3 kpc region. Model  $B$  is more dominated by the disk component: the crossing point of the disk and dark matter is at 9 kpc.

**Table 1.** Initial parameters of models

| Parameter   | $A_1$ and $A_2$       | $B$                  |
|---|-----------------------|----------------------|
| Disk Mass ( $M_\odot$ )                           | $4.28 \times 10^{10}$ | $6.0 \times 10^{10}$ |
| Total Mass ( $M_\odot$ )                          | $2.04 \times 10^{12}$ | $1. \times 10^{12}$  |
| Disk exponential length (kpc)                     | 3.5                   | 3.0                  |
| Disk exponential height (kpc)                     | 0.25                  | 0.25                 |
| Stability parameter $Q$                           | 1.2                   | 1.3                  |
| Halo concentration after baryonic contraction $C$ | 15                    | 15                   |
| Total number of particles                         | $3.55 \times 10^6$    | $7.8 \times 10^5$    |
| Number of disk particles                          | $2 \times 10^5$       | $1.1 \times 10^5$    |
| Particle mass ( $M_\odot$ )                       | $2.14 \times 10^5$    | $5.45 \times 10^5$   |
| Formal maximum resolution (pc)                    | 22                    | 43.6                 |

gross properties (e.g., the maximum circular velocity and the stellar surface density at 8.5 kpc) are not far from what is observed in our Galaxy. This is why we scale different physical quantities to astronomical units (kpc,  $M_\odot$ , and so on).

### 2.3 Numerical simulations

We use the Adaptive-Refinement-Tree (ART)  $N$ -body code (Kravtsov et al. 1997; Kravtsov 1999) to run the numerical simulations analyzed in this paper. The code starts with a uniform grid, which covers the whole computational box. This grid defines the lowest (zeroth) level of resolution of the simulation. The standard Particles-Mesh algorithm is used

to compute the density and gravitational potential on the zeroth-level mesh with periodical boundary conditions. The code then reaches high force resolution by refining all high density regions using an automated refinement algorithm. The refinements are recursive. A refined region can also be refined. Each subsequent refinement level has half of the previous level's cell size. This creates a hierarchy of refinement meshes of different resolution, size, and geometry covering regions of interest. Because each individual cubic cell can be refined, the shape of the refinement mesh can be arbitrary and effectively match the geometry of the region of interest. This algorithm is well suited for simulations of a selected region within a large computational box, as in the simulations presented below.

The criterion for refinement is the local density of particles. If the number of particles in a mesh cell (as estimated by the Cloud-In-Cell method) exceeds the level  $n_{\text{thresh}}$ , the cell is split ("refined") into 8 cells of the next refinement level. The refinement threshold depends on the refinement level. The threshold for cell refinement was low on the zeroth level:  $n_{\text{thresh}}(0) = 2$ . Thus, every zeroth-level cell containing two or more particles was refined. The threshold was higher on deeper levels of refinement:  $n_{\text{thresh}} = 3$  and  $n_{\text{thresh}} = 4$  for the first level and higher levels, respectively.

During the integration, spatial refinement is accompanied by temporal refinement. Namely, each level of refinement is integrated with its own time step, which decreases by factor two with each refinement. This variable time stepping is very important for accuracy of the results. As the force resolution increases, more steps are needed to integrate the trajectories accurately. Extensive tests of the code and comparisons with other numerical  $N$ -body codes can be found in Kravtsov (1999) and Knebe et al. (2000). The current version of the ART code has the ability to handle particles of different masses. In the present analysis this ability was used to increase the mass (and correspondingly the force) resolution inside a region centered around the simulated galaxy.

The simulations presented here are run using  $128^3$  zeroth-level grid in a computational box of 2.86 Mpc. Model  $A_1$  is simulated for  $5.2 \times 10^9$  yrs with 336 zero-level time steps. The code reached 10 refinement levels and had about 9 million cells. The number of time steps at the highest resolution level was about 344,000, which gives the time step of  $1.5 \times 10^4$  yrs. With this time step it takes 3500 steps to make one orbital period at the 3 kpc radius. The formal spacial resolution – a cell size at the 10th level – is 22 pc. At about twice that value the force is close to the Newton's law. Central 6 kpc region was resolved with cells of the size not more than 100 pc. Model  $A_2$  had similar parameters, but it was simulated for 6.2 Gyr.

Model  $B$  was simulated with a smaller time step of  $1.02 \times 10^4$  yrs (at the 9th level) for  $4.5 \times 10^9$  yrs. It reached the highest resolution of 43.6 pc, but because of fewer particles, the volume with high resolution was significantly smaller than in models  $A$ : there were only 3.9 million cells in model  $B$ . The number of steps at the highest 9th level was  $4.4 \times 10^5$ .

It is interesting to compare our numerical simulations with those presented in Debattista & Sellwood (1998, 2000) and with more recent simulations of Athanassoula & Misiriotis (2002). It is straightforward to compare the resolution

of our simulations with that in Debattista & Sellwood (1998, 2000) because we use the same Particle-Mesh algorithm. The formal (one cell) resolution in their simulations was 1/5 of the disk scale length. If we scale the length to 3.5 kpc, than we get the formal resolution of 700 pc, which is 30 times larger than in our models. Athanassoula & Misiriotis (2002) used the TREE code with the Plummer softening of 0.0625 of the disk exponential length. Again, scaling it to 3.5 kpc, we get 220 pc. The force of gravity comes close to the Newton's law at approximately three Plummer softening lengths or at 660 pc. In our models this scale is 40-80 pc in the center and is 200 pc for the entire 6 kpc region.

## 2.4 Finding the bar

We follow Debattista & Sellwood (2000) and Athanassoula & Misiriotis (2002) when finding bars in our simulations. We start with finding the center of the system. This can be done in different ways. Debattista & Sellwood (2000) minimized the sum of distances of all particles relative to a center. We used a more simple algorithm: the center of mass of stellar particles. We then bin stellar particles using cylindrical shells spaced equally in logarithm of the distance. For each bin we find the Fourier components of second harmonic of the angular distribution of particles:

$$a_2 = \frac{1}{N} \sum_{i=1}^N \sin(2\phi_i), \quad b_2 = \frac{1}{N} \sum_{i=1}^N \cos(2\phi_i), \quad (10)$$

where  $N$  is the number of stellar particles in the bin and  $\phi_i$  is the angle of the  $i$ -th particles. We then find the phase and the amplitude of the second harmonic  $A_2^2 = (a_2^2 + b_2^2)/2$ .

Except for the very early stages of evolution, when the bar was just emerging, it is easy to identify the bar. In the central region the amplitude of the second harmonic  $A_2$  changes gradually from bin to bin and its phase  $\phi$  is almost constant. At larger distances (typically larger than 5 kpc) the amplitude declines and the phase shows large variations. In the very centre the shot noise complicates the results. Because of these considerations, we use bins with radii in the range 0.5–3 kpc to find the amplitude and the phase of the bars. We find the bar amplitude and its phase as the amplitude-weighted means at different radii:  $\langle A_2 \rangle = \sqrt{\langle A_2^2 \rangle}$ ,  $\langle \phi \rangle = \langle \phi A_2 \rangle / \langle A_2 \rangle$ . When finding the average amplitude and the phase, we exclude bins with  $A_2$  less than 1/2 of the maximum amplitude found in the range of the radii. Once the phase of the bar is found at different moments of time, we estimate the frequency of bar rotation (the pattern speed) by numerical differentiation:  $\Omega_p = d\phi/dt$ .

Finding the radius of the bar is a more difficult problem because bars do not have clear boundaries. Discussion of different methods of finding the bar major axis can be found in Debattista & Sellwood (2000) and in Athanassoula & Misiriotis (2002). We use two different methods, each being sensible and producing reasonable, but slightly different results. We find the surface density along and perpendicular to the bar. We then define the radius of the bar as the radius at which the surface density along the bar is twice of the surface density at the same distance perpendicular to the bar. In the second prescription the bar radius is defined as the radius at which the contours of the surface density have axial ratio of two. We also tried other prescriptions, which are

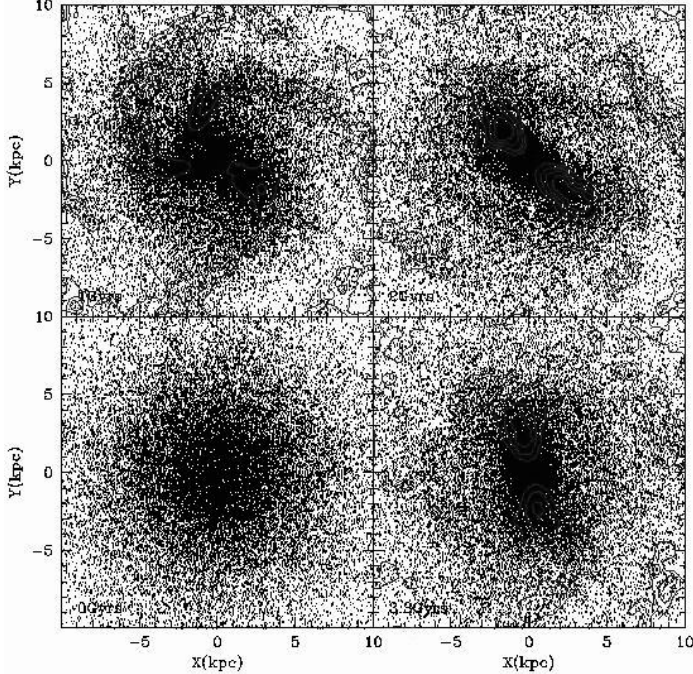


**Figure 2.** Distribution of the stellar component at different stages of evolution for model  $A_1$ . Starting from the left bottom panel in the clock-wise direction the panels correspond to the initial moment; 1 Gyr; 2 Gyr; 3.3 Gyr. The disk rotates counter-clockwise. To avoid crowding we show only every fifth particle. At the distance 5 kpc the disk made 20 orbital periods during 3.3 Gyr.

to some degree reminiscent to what was used by Debattista & Sellwood (2000). We find the major semi-axis as the radius at which either the phase of the bar starts to deviate by more than 10 degrees or as the radius at which the amplitude falls below 1/2 of its maximum value. We find that typically the prescriptions based on the surface density give the same results as those based on the amplitude and the phase of the bar. For example, for model  $A_2$  at  $t = 6.2$  Gyrs the bar radii are:  $R_{\text{bar}} = 4.3$  kpc ( $A_{2,\text{max}}/2$ ),  $= 5.5$  kpc ( $\Delta\phi = 10^\circ$ ),  $= 4.2$  kpc ( $\Sigma_{\text{major}}(r_{\text{major}}) = 2\Sigma_{\text{minor}}(r_{\text{major}})$ ),  $= 5.3$  kpc ( $\Sigma_{\text{major}}(r_{\text{major}}) = \Sigma_{\text{minor}}(r_{\text{major}}/2)$ ). Here  $\Sigma_{\text{major}}(r)$  and  $\Sigma_{\text{minor}}(r)$  are the stellar surface densities along the major and the minor axes respectively. Nevertheless, we find that the surface densities give more stable results because occasionally spiral waves in the outer disk align with the bar and the amplitude/phase conditions produce spurious results.

We present the total range of the bar sizes produced by the two methods based on the surface density profiles. The estimates vary by 20–30 percent. We would like to emphasize that every estimate was reasonable: the estimates in the middle of the range are no better than the extremes.

### 3 EVOLUTION

Figure 2 shows the evolution of the stellar component in model  $A_1$ . Because the system is relatively hot and the dark matter is significant in the central region, the bar develops slowly. After 1 Gyr after the beginning (top left panel) the bar has not yet appeared. Nevertheless, extended spiral arms

are clearly present in the disk. At that time the system has already made many rotations: at the distance of 5 kpc one orbital period is equal to  $T \approx 1.6 \times 10^8$  yr. The bar develops after 2 Gyrs (top right panel). At that moment its radius is  $\approx 4 - 5$  kpc. The spiral arms can still be seen, but they start to get weaker after that. At the last shown moment (3.3 Gyr) only fragments of spiral arms can be detected. The bar is still very strong, but its amplitude is visibly smaller than at the peak at 1.8 Gyr. The bar gradually grows with time. At the last moment (5.2 Gyrs) the major semi-axis of the bar is  $\approx 6$  kpc. The evolution of model  $B$  is qualitatively the same, but it is more violent and is faster than in the case of model  $A_1$ . The evolution is also faster in the case of the colder model  $A_2$ . The evolution of model  $A_2$  is very different. A short (1 – 1.5 kpc) bar forms around 1 Gyr after the beginning. The bar was gradually increasing its length. After almost 3 Gyrs from the beginning the bar started to grow in length. Its amplitude also increased significantly.

Formation of bars is accompanied by significant redistribution of the stellar mass. Even a visual comparison of the bottom panels in Figure 2 shows that the central surface density increases. Figure 3 shows the evolution of the fraction of stellar mass inside given radius. The total mass inside 5 kpc practically does not change with time. All the mass exchange happens inside the central 1-2 kpc, where it is very strong. For example, the stellar mass inside the central 1 kpc region increases by a factor 4 by the end of evolution. Note that the time-scale of the evolution is about twice as short in the case of the more disk-dominated model  $B$  and for the colder model  $A_2$ .

Bottom panels in Figure 4 present more detailed information on the change in the densities. In the central 2 kpc the ratio of the stellar density to the dark matter density have increased by a factor of two by the end of the evolution. As the result, even model  $A_1$  became significantly baryon-dominated in the center. The Figure also shows that the central growth of the density goes at the expense of the stellar density in the middle part (2–8 kpc). At those radii the final baryon-to-dark matter ratio was a bit surprising: it went down producing dark-matter dominated disk. This effect is more pronounced in model  $B$ , which was initially more baryon-dominated than models  $A$ .

The dramatic changes of the disk component hardly affected the dark matter: it stayed almost unchanged. There was a 10-20 per cent increase of the dark matter density in the central 2 kpc region. The rest of the halo was practically unaffected.

Because of the violent processes in the central region, one would naively expect to find a very strong heating of the disk in the central part and much less in the outer parts. One of the ways to characterize the “hotness” of disk is the ratio of the rotational velocity  $V_\phi$  to the velocity dispersion  $\sigma_\phi$ . The top plots in the Figure 4 show just an opposite trend: the heating is stronger in the outer part of the disk. A possible explanation for this is the heating by spiral waves, which appeared in the outer parts of the disk. Large amplitude spiral waves produce non-circular motions and increase the azimuthal dispersion. After the waves die out, they leave behind a hotter disk.

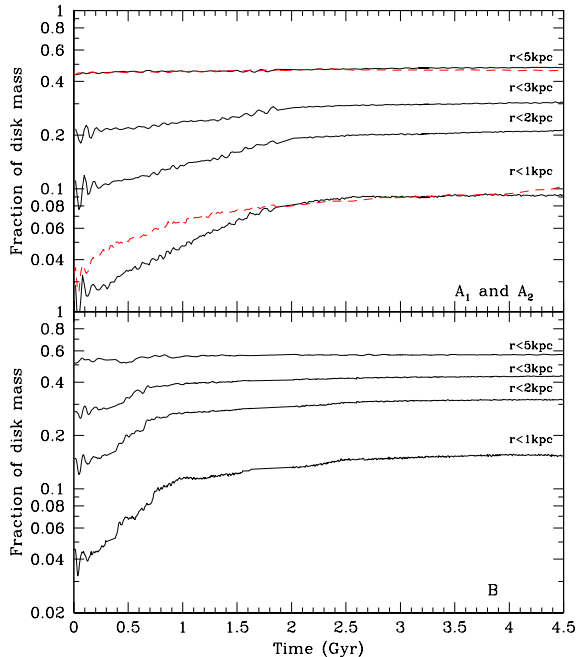


**Figure 3.** Evolution of fraction of disk mass inside given radius. The top panel is for models  $A_1$  (full curves) and  $A_2$ . The bottom panel shows model  $B$ . The total mass inside 5 kpc practically does not change with time. Most of the mass exchange happens inside the central 1 – 2 kpc. The disk mass inside the central 1 kpc region increased by a factor 4 by the end of evolution. The time-scale of evolution is about twice shorter in the case of the more disk-dominated model  $B$  and the colder model  $A_2$ .

#### 4 ANGULAR MOMENTUM

Formation of a bar is accompanied and even may be driven by the exchange of the angular momentum between different components of the system. The exchange of the angular momentum between the quickly rotating stellar component and the non-rotating dark matter is of special interest because it is often used as one of the arguments against a presence of a significant amount of the dark matter in the central parts of galaxies. Numerically it is a challenge to simulate the two-component system: any artificial numerical coupling will result in a transfer of some angular momentum from the stellar to the dark matter component. Without the bar the system is axisymmetric and no transfer should happen. Once the bar or any other non-axisymmetric perturbation forms, the dark matter should react to it by generating a wake behind the perturbation, which must result in a transfer of the angular momentum to the dark matter. The exchange of the angular momentum is not limited by the disk-dark matter interaction. The stellar component also experiences the exchange between different parts of the disk, which we find to be much more important for the evolution and for the structure of bars.

Figure 5 presents the evolution of the z-component of the angular momentum of the stellar component (disk + bar) for all the models. Figure 6 shows details of the evolution for  $A_1$  and  $B$  models. Model  $A_2$  shows results similar to model  $A_1$ . The total stellar angular momentum clearly is declining with time, but the rate of the decline is very small. After 4.5 Gyrs the change was  $\approx 5\%$ . This level of

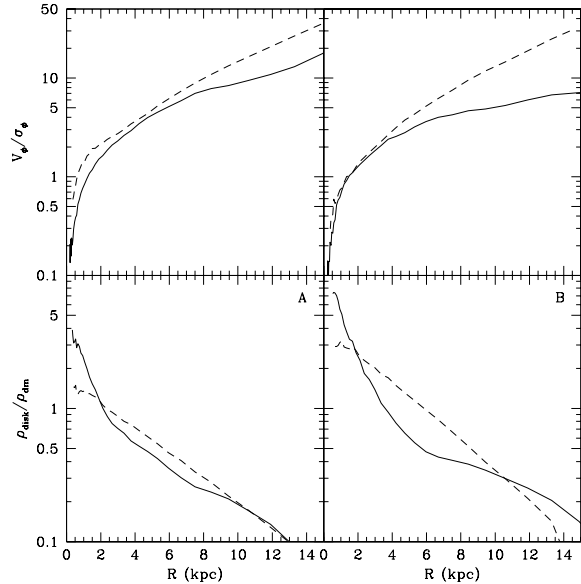


**Figure 4.** The baryon-to-dark matter ratios (bottom panels) and the ratio of the rotational velocity to the velocity dispersion (top panels) for model  $A_1$  (left panels) and model  $B$  (right panels). The dash curves show the initial models. The final models are shown with full curves. The central growth of the density goes at the expense of the stellar density in the middle 2 – 8 kpc region. At those radii the final baryon-to-dark matter ratio went down producing dark-matter dominated disk. The top panels show that the heating of the disk preferentially happens in the outer regions outside of the bar. Spiral waves may cause the heating.

the angular momentum loss is at odds with the results of Debattista & Sellwood (2000), who find about 40% decline.

It was interesting to find that the specific angular momentum  $L_z$  at different radii also shows very little evolution. Only at the very centre the angular momentum declines slightly. The specific angular momentum is practically constant at larger radii. At first sight this indicates that the distribution of the angular momentum does not evolve. This is not true. Figure 3 shows that the stellar mass in the central region increases quite substantially. Because the specific angular momentum  $L_z(r)$  at a given radius does not change, this mass increase implies that the stellar particles, which accumulate in the central region, actually lose their angular momentum. This is clarified by Figure 7, which shows significant changes in the distribution of the angular momentum of the stellar particles in the course of the evolution. The changes are especially noticeable at low  $L_z$ : a large peak forms. The peak at very low (almost zero) angular momentum is produced by the particles, which are located in the central region. The peak is produced by particle which initially had intermediate angular momentum and lost some of their rotation during bar formation. As the result of this migration of particles the distribution of  $L_z$  at later moments has a deep at intermediate angular momenta. The number of particles at large  $L_z$  increases, which is more clearly seen in the case of model  $B$ .

Evolution of the  $L_z$  distribution is not gradual. Most of the changes occur before and during the bar formation. Model  $B$  clearly shows that once the bar has formed (after 1 Gyr of evolution) the distribution experiences very little

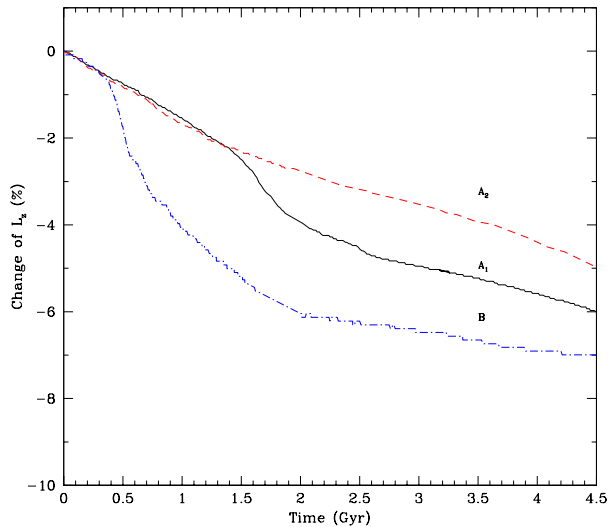


**Figure 5.** Evolution of angular momentum of disks in different models. In all cases the angular momentum declines due to the dynamical friction with the dark matter. The decline is very small – only few percent for  $\sim 5$  Gyrs of evolution.

evolution. This indicates that the bar itself does not lead to a significant exchange of the angular momentum between the particles. Most of the evolution is done not by the bar, but by the processes, which produce the bar. Nevertheless, the evolution does not stop after the bar forms. It proceeds, but with much lower rate.

Because of the large moment of inertia of the dark matter, it is difficult to detect small changes in the distribution of the angular momentum of the dark matter particles. The largest effect was found in the central region. By the end of the evolution the dark matter in the central 2 kpc region rotated with velocity  $3 - 7 \text{ km s}^{-1}$ . This rotation has very little dynamical effect. Figure 8 presents an example of the change of the angular momentum of the  $z$ -component of the specific angular momentum of 10,000 particles, which initially were in a shell centered at 3 kpc from the centre. The change in the angular momentum is clearly detected, but it is very small.

To summarize, we clearly find indications of the dynamical friction between the dark matter and the stellar component. Nevertheless, the amount of the angular momentum lost by the stellar particles is very small: about 5% during 5 Gyrs of evolution. There is much larger exchange of the angular momentum between stellar particles. Most of this exchange happens during the formation of the bar. Once the bar is in place, the distribution of the angular momentum changes very little.

## 5 STRUCTURE OF BARS: THE PATTERN SPEED AND THE SURFACE DENSITY

Figures 9 and 10 show the evolution of the pattern speed and the amplitude of the bars in our simulations. Models

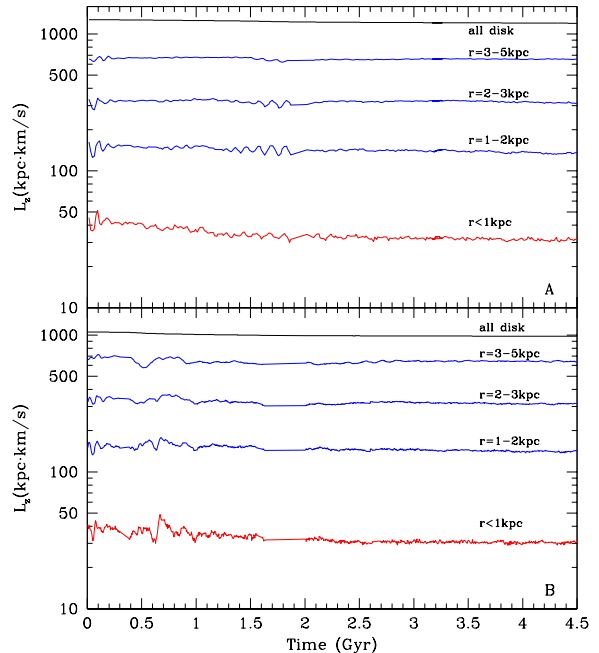


**Figure 6.** Evolution of the specific angular momentum of the disk for the  $A_1$  (top panel) and the  $B$  (bottom panel) models. The top curves in each panel show that the total angular momentum of disk particles declines very little – few per cent after 4.5 Gyrs of evolution. The other curves present an average specific angular momentum for disk particles inside spherical shells indicated in the plot. Only the very central region (radius less than 1 kpc) exhibits some decrease (a factor of 1.5) of angular momentum. Outside the very center the specific angular momentum does not change.

$A_1$  and  $B$  evolve qualitatively similar. After some initial period (different for models  $A_1$  and  $B$ ) a bar forms, which after that rotates with almost constant speed. The amplitude of the bar in the model  $B$  experienced a noticeable decline (a factor of two) at 2 Gyrs. This change in the amplitude was not accompanied by any other obvious changes. For example, the pattern speed did not change. The bar pattern speed is slightly larger in model  $B$  ( $\approx 33 \text{ km s}^{-1}/\text{kpc}$ ) as compared with model  $A_1$  ( $\approx 27 \text{ km s}^{-1}/\text{kpc}$ ). What is remarkable about the pattern speeds is that they are almost constant. The evolution of model  $A_2$  is very different. For the first 3 Gyrs the bar was very quickly rotating with the pattern speed of  $\approx 50 \text{ km s}^{-1}/\text{kpc}$  – almost twice larger than in model  $A_1$ . At later moments the pattern speed was declining. It went down to  $\approx 25 \text{ km s}^{-1}/\text{kpc}$  by the end of evolution.

In order to find how fast is the bar rotation, we show in the Figure 11 the bar pattern speeds and the the rotation and the circular velocity curves of the models. The thick horizontal bars in the plots indicate the length of the bars. The corotation radius can be identified as the radius of intersection of the bar pattern speed with the rotation curve. In all three models the bars rotate fast with the ratio of the corotation radius to the bar length equal to  $\mathcal{R} \approx 1.2 - 1.7$ .

Figure 12 shows the surface density profiles of the stellar components in the models. The surface density profiles seems to indicate a development of normal galactic compo-

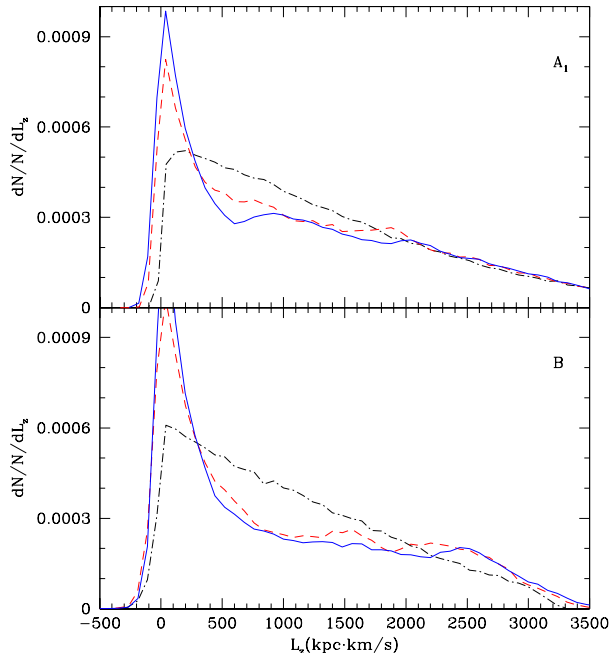


**Figure 7.** Distribution of the z-component of the angular momentum of the stellar particles for models  $A_1$  (top panel) and  $B$  (bottom panel) at different moments of time. Initial distribution is shown by dot-dashed curves. Particles with low angular momentum are preferentially at small radii. Large angular momentum is coming from particles at large distances. Dotted curves are for 1-1.5 Gyrs after the beginning of the evolution. The final distribution (4.5-5 Gyrs) is qualitatively the same for both models. The peak at small angular momenta corresponds to the bar. The number of particles with intermediate angular momenta substantially decreased. There is an excess of particles with very large angular momentum. The changes in the distribution are much stronger in the case of model  $B$ , which had less dark matter and had more massive disk.

nents: an exponential disk and a (exponential) bulge. Note that even after significant evolution in the central part, the outer part the disk (radii larger than 5 kpc) is still well approximated by a simple exponential profile. Still, there is a change even in the outer part: the exponential scale-length increases quite substantially - by a factor of 1.5.

## 6 DISCUSSION

Bars in our models are different from what was found in simulations of Debattista & Sellwood (2000). In two of our dark matter-dominated models bars do not show a strong tendency to slow down. This contradicts results of Debattista & Sellwood (2000), who always find that the pattern speed of bars substantially declines with time. We tried to find an explanation for the disagreement. Numerical effects is an obvious first suspect. The force resolution in the Debattista & Sellwood (2000) models was more than an order of magnitude lower than in our simulation. In an effort to reproduce at least some conclusions of Debattista & Sellwood (2000), we re-run model  $A_1$  with the resolution comparable with that in models of Debattista & Sellwood (2000). The evolution was so much affected by the lack of the resolution

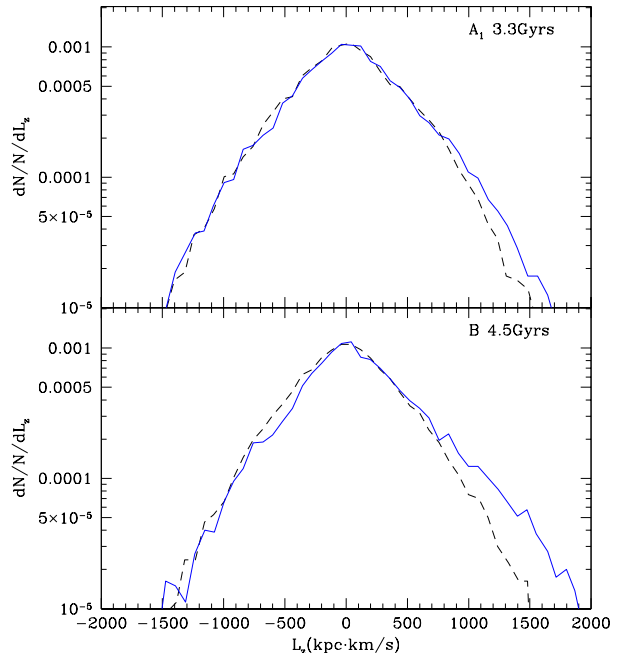


**Figure 8.** Distribution of z-component of the angular momentum of dark matter particles at different moments. Dashed and full curves are for initial and advanced moments (3.3 Gyrs for  $A_1$  and 4.5 Gyrs for  $B$ ) of evolution. We present results only for 10000 particles, which initially were in a spherical shell centered at 3 kpc. Particles at other radii showed even smaller effects. The changes in the angular momentum are clearly seen in both models: there are more particles with high angular momentum. This indicates that the dynamical friction transfers some angular momentum to the dark matter, but the effect is extremely weak.

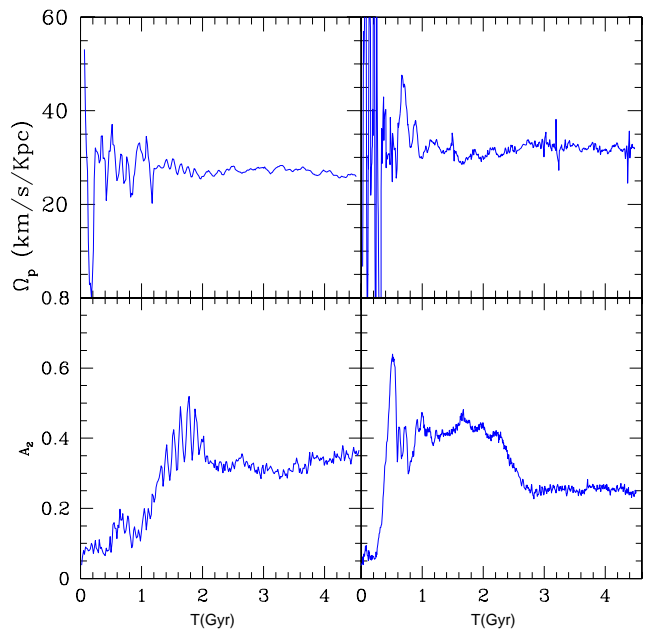


**Figure 9.** Evolution of the bar amplitude (bottom panels) and the pattern speed (top panels) for the models  $A_1$  (left panels) and  $B$  (right panels)

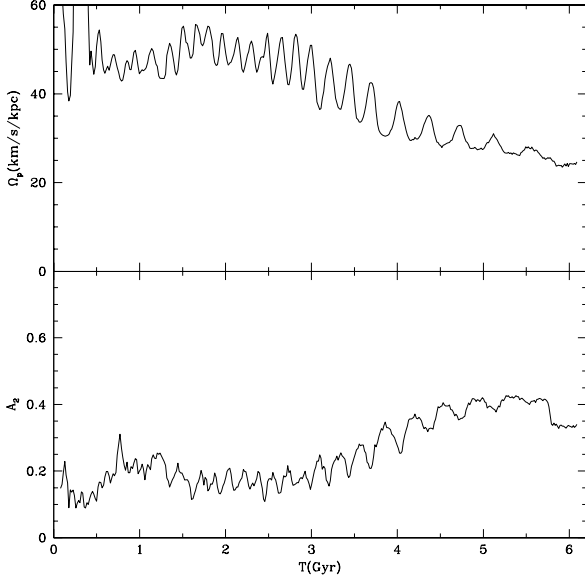


**Figure 10.** Evolution of the bar amplitude (bottom panel) and the pattern speed (top panel) for model  $A_2$ .

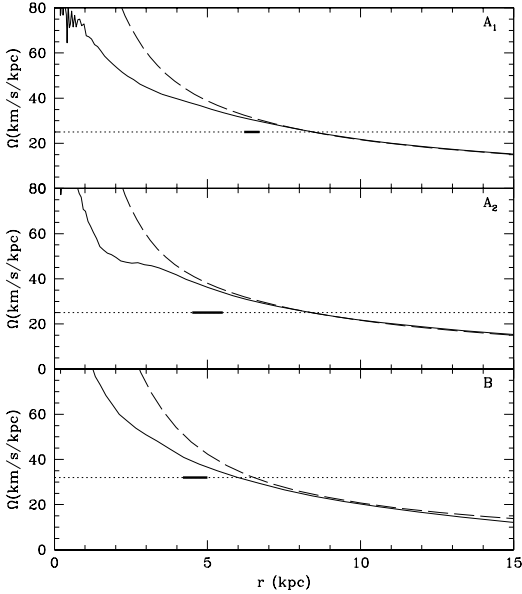


**Figure 11.** Different frequencies in models  $A_1$ ,  $A_2$ , and  $B$ . The full curves show the frequency of rotation of the disk  $\Omega_{\text{rot}} \equiv V_\phi/R$ . The dashed curves present the frequency of rotation for a cold disk  $\Omega_{\text{circ}} \equiv \sqrt{GM/R^3}$ . The difference between the two frequencies are due to the asymmetric drift. The dotted horizontal lines show the frequency of rotation of the bars. The extension of the bars in the models is indicated by the thick lines. The distance of a bar from the rotation curves is a measure of how fast is the bar. The bar in the model  $B$  is clearly a very fast bar, which extends almost up to the corotation. The bars in models  $A$  rotate slower, but they are still fast bars.

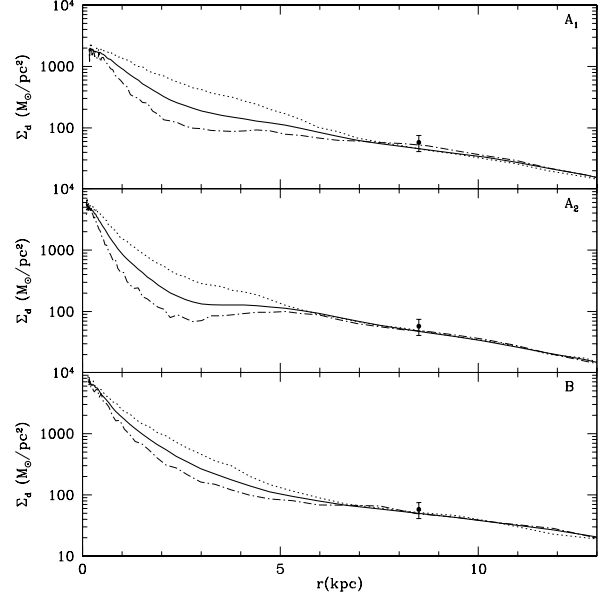


**Figure 12.** Surface density profiles of the stellar components for models  $A_1$ ,  $A_2$ , and  $B$ . The full curves present the azimuthally averaged profiles. Dashed curves show double exponential fits with parameters presented in the plots. The dotted curves show the surface density along the major axes of the bars. The surface densities along the minor bar axis are shown with the dot-dashed curves. All the curves are obtained by averaging over three time moments covering about 0.5 Gyr. For comparison a large dot shows the surface density of the disk (stars + gas) for our Galaxy at the solar position.

that after running the model for more than 2 Gyrs and not finding even a hint of a bar, we abandoned the simulation. We then re-started the simulation with decreased “thermal” velocities in the disk. The  $Q$  parameter was set at the value  $Q = 0.05$  used by Debattista & Sellwood (2000). In this simulation a bar forms. Figure 13 shows that the pattern speed decreases very substantially over a relatively short period of time - more or less in line with what was found by Debattista & Sellwood (2000). Thus, we find the same behavior of bars – declining pattern speed – if we substantially reduce the resolution and reduce the random velocities of disk particles. The angular momentum of the stellar particles also was declining faster than in the high resolution run. This exercise clearly demonstrates that the force resolution is an important factor. In our simulations the low force resolution produced erroneous results that the bar pattern speed declines with time. The “coldness” of the disk may also have affected the pattern speed.

Length is another important property of bars. In our simulations bars have radii comparable to the exponential disk length. This is quite different from what, for example, Athanassoula & Misiriotis (2002) find. The bar length in their models is more than three times longer than the disk scale-length. They also find that the bar length is larger for models with larger dark matter mass. Bars are also very long in the models of Debattista & Sellwood (2000): they span entire disk. In order to test how numerical resolution may affect the bar length, we rerun model  $A_2$  with lower resolution comparable to the resolution of Athanassoula & Misiriotis (2002). Figure 14 shows the distribution of stellar particles

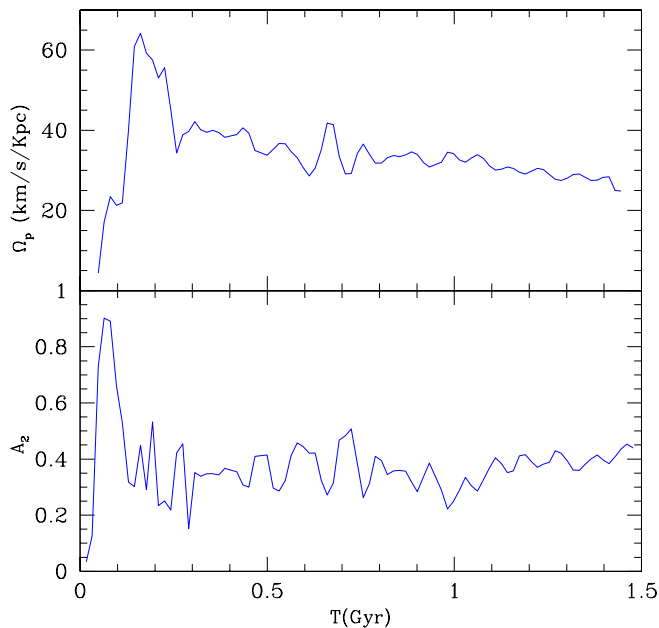


**Figure 13.** Evolution of the pattern speed and the bar amplitude in a simulation with initially cold disk with  $Q = 0.05$ . Other parameters of the simulation are the same as for model  $A_1$ . The simulation was done with a very low resolution of 0.5 kpc to mimic results of Debatista & Sellwood (2000). In this case the pattern speed quickly decreases with time giving an impression that the bar is slowed down by the dynamical friction with the dark matter. This “slowing down” of the bar is an artifact of unrealistically cold disk and grossly insufficient force resolution.

of the simulations for model  $A_2$  at different moments of time. The system was clearly affected by the resolution. At 2 Gyrs the bar is barely visible in the high resolution run, but it is much longer and stronger in the low resolution run. The differences are not as large at later moments, but even at later moments the differences are substantial. This example shows that the bar length is quite sensitive to the effects of the resolution. Short bars are also formed in high resolution simulations of Sellwood (2002).

We may only speculate why a better force resolution leads to shorter and weaker bars. Orbital resonances are traditionally blamed for the growth of bars. Fast rotating bars trap particles. This in turn increases the strength of the bar. It gets longer and more massive trapping even more trajectories. Low force and high mass resolutions make the system more resonant by producing gravitational potential with too shallow gradients. Motion of particles in such potentials can be more susceptible to resonances. Thus, we get longer bars. Increased forced resolution results in steeper gradients of the density and the potential. As the result, particle trajectories do not stay as much in the resonances, which decreases the rate of the growth of the bar. The comparison of the low and high resolution runs of the model  $A_2$  gives a support to this picture.

Numerical effects are clearly important for the structure of the system. Still, they can not explain all the differences between our results and those of Athanassoula & Misiriotis (2002). The bar in the low resolution run of  $A_2$  model

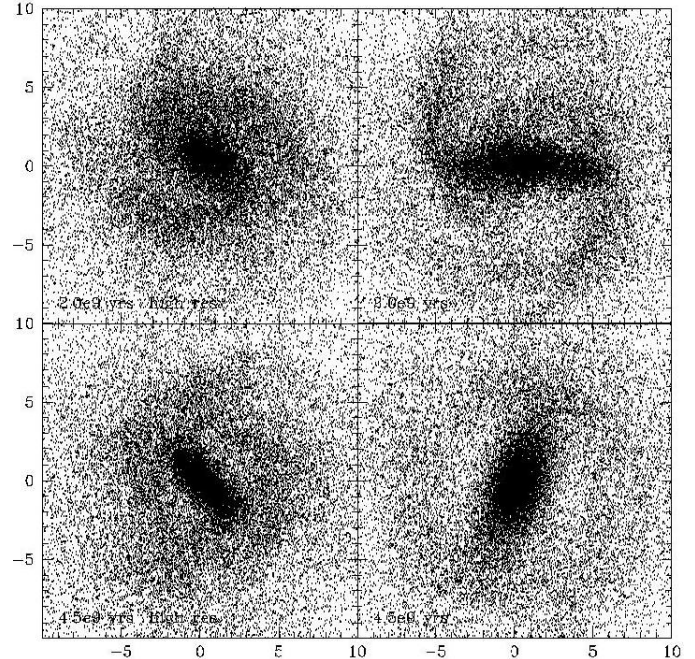


**Figure 14.** Effects of resolution on bar formation in model  $A_2$ . Left panels show stellar particles in the simulation, which reached 20 pc resolution. Right panels show the same model simulated with the resolution limited to 350 pc. The top panels are for 2 Gyrs after initial moment; the bottom panels are for 4.5 Gyrs. The high resolution run has a very short (1 kpc) bar for 3 Gyrs, while the low resolution run has remarkably strong and long bar from the very beginning. Axes are labeled in units of kpc. This figure illustrates that numerical resolution can significantly affect structure of a bar. Lack of resolution results in longer and stronger bars.

is longer than in the high resolution run. Still, it is shorter than what was found by Athanassoula & Misiriotis (2002). The remaining differences likely are due to the differences in the overall structure of the system. Our halo was significantly more extended (250 kpc as compared with 50 kpc in Athanassoula & Misiriotis (2002)). The halo density profile in our model was shallower in the central 20 kpc region resulting in larger rms velocities of particles. Our disk was slightly “hotter”. Our estimates show that each individual effect is not strong enough to explain the differences in the bar length. Yet, each effect points in the same direction: systems studied by Athanassoula & Misiriotis (2002) are more susceptible to resonances. The effects accumulate over billions of years producing longer bars in the Athanassoula & Misiriotis (2002).

It is a matter of debate which initial setup was more realistic. Our halos are consistent with predictions of the cosmological models. They extend to the virial radius; they have realistic profiles. Halos in Athanassoula & Misiriotis (2002) simulations present mostly historical interest. In any case, we do not confirm Athanassoula & Misiriotis (2002) conclusions that bars in models with centrally concentrated dark matter are longer (3-4 disk exponential lengths) than in the maximum disk models. At best, their results are valid only for the particular models they studied. They are not valid as a general statement that realistic models should have long bars. We also believe that results of Athanassoula

& Misiriotis (2002) were significantly affected by numerical effects.

It is an interesting question how a bar can possibly *not* slow down when it rotates inside a dense dark matter halo. Even in model  $A_1$  the disk lost 6 percent of its angular momentum after 5 Gyrs of evolution. One should expect that most of the loss comes from the bar. Because the bar has only 40% of the stellar mass, one expects that the bar should lose around 15% of its angular momentum. This is still marginally consistent with the behaviour of the pattern speed in Figure 9. Still, what if  $\Omega_p$  is really constant? Can a bar rotate with the constant speed and lose its angular momentum? If we believe the arguments presented by Weinberg (1985), the answer is “No”. Indeed, if a solid rotating bar, often used in these kind of estimates (Weinberg 1985; Little & Carlberg 1991; Weinberg & Katz 2001), loses its angular momentum, it *must* slow down. Yet, real bars may behave differently because they are not solid objects. Bars are made of particles, which stream through them creating a wave pattern, which we call a “bar”. When the bar loses angular momentum, it is individual particles which lose it. The particles can move to orbits with smaller radii where orbital frequency is larger. It is reasonable to assume that the bar speed is proportional to the orbital frequency of particles. Because the particles rotate with larger frequency, the bar can speed *up* when it loses the angular momentum. Real bars have another feature, which complicates things even more. Typically, they have a tendency to grow. For example, the bar in model  $A_1$  has increased its length from  $\approx 4 - 5$  kpc at 3 Gyrs to  $\approx 6 - 6.5$  kpc at 5 Gyrs. This 30% increase in the bar length is due to particles, which came from large radii. Because the rotation curve is nearly flat, particles at larger radii have smaller orbital frequencies. When they “join” the bar, it will have a tendency to slow down. This happens if the particles do not significantly change trajectories. If the particles lose their angular momentum and decrease average radius, they may cause the bar to speed up.

The outcome of all these competing processes is difficult to predict. We find that slow growing bars rotate with almost constant speed (e.g., bars in models  $A_1$ ,  $B$ , and the bar in model  $A_2$  at  $t < 3$  Gyrs). If a bar grows fast, it significantly decreases its pattern speed. This happened in model  $A_2$  at  $t = 3 - 4$  Gyrs. At 3 Gyr the bar was very short ( $\sim 1.5$  kpc) and weak. At earlier moments of time it was growing very slowly and was rotating with high constant speed for almost 3 Gyrs. At  $t \approx 3$  Gyrs the bar starts to grow very fast. By the end of evolution (6 Gyrs) it was 4.5 – 5 kpc long and it slowed down by a factor of two. Its Rparameter was smallest for all the cases we studied.

## 7 CONCLUSIONS

We study formation of bars in galactic models with equilibrium exponential disks rotating inside extended dark matter halos predicted by modern cosmological models. The amount of the dark matter in the central 10 kpc region is substantial - it is larger than the disk mass. Our models have parameters, which approximately match those of the Milky Way galaxy: the virial mass is  $(1 - 2) \times 10^{12} M_\odot$ , the total mass of the disk and the bulge is  $(4 - 6) \times 10^{12} M_\odot$ . Dark matter halos in our models extend to the virial radius

of 200-300 kpc. We use millions of particles to simulate the models.

We find that the dynamical friction between the dark matter and the bar results in some transfer of angular momentum to the dark matter halo, but the effect is much smaller than previously found in low resolution simulations and is incompatible with early analytical estimates. The mass and the force resolutions are crucial for the dynamics of bars. In simulations with the low resolution of 300-500 pc we find that the bar slows down and the angular momentum is lost relatively fast. In simulations with millions of particles, which reach the resolution of 20-40 pc, the pattern speed may not change over billions of years and the stellar component loses very little (5 – 10%) of its total angular momentum.

Bars in our models are fast rotators with the ratio of the corotation radius to the bar major semi-axis being in the range  $\mathcal{R} = 1.2 - 1.7$ , which is marginally compatible with observational results. The initial random velocities of the disk in the central  $\approx 1 - 2$  kpc region can substantially affect the structure of bars. In our simulations “hot” disks develop a longer bar, which rotates at an almost constant pattern speed. Colder models generate an initially shorter bar, which grows and slows down.

In contrast to many previous simulations, bars in our models are relatively short. As in many observed cases, the major bar semi-axis in the models is about an exponential length of the disk.

The transfer of the angular momentum plays a very important role in the secular evolution of the disk and the bar, but it is not the transfer between the stellar component and the halo. The main effect is the angular momentum transfer from the central part of the disk/bar to the outer disk. This transfer leads to a substantial increase of the stellar mass and to a decrease of the dark matter-to-baryons ratio in the centre of the galaxy. For the Milky Way- scale models the central 2 kpc is strongly dominated by the baryonic component after 1 – 2 Gyrs since the onset of the instability. At intermediate 3 – 10 kpc scales the disk is sub-dominant: spherically average density of the disk is 2-3 times smaller than the density of the dark matter. This makes an interesting twist for the never ending debate between supporters and opponents of the maximum disks. For the barred galaxies (or galaxies, which were barred) both groups are right: the central part is the maximum disk (maximum bulge or bar, to be more precise), but the outer part is the sub-maximum disk. Another effect of the bar formation is the increase by a factor of  $\approx 1.2 - 1.5$  of the exponential length of the disk. This may change theoretical predictions for the disk lengths in hierarchical models.

We find that the surface density profile of an evolved system is well approximated by a double exponential law. The 1/4 law for the bulge gives a worse fit, but it is not excluded. Only in extreme cases (very late stages of evolution, very strong bars formed in low resolution simulations) we see a tendency for a bar to produce a flat part of the surface density in the interface of the bar and the disk.

To summarize, we use more realistic models than in most of previous simulations and find that the models with substantial amount of the dark matter produce bar structure in striking agreement with observational results.

**ACKNOWLEDGMENTS**

We thank J. Sellwood for exciting discussions and for showing us his preliminary results. We are grateful to N. Vogt for her comments. We thank the Center for Cosmological Physics, University of Chicago, for hospitality and support. We acknowledge support from the grants NAG- 5- 3842 and NST- 9802787 to NMSU. Computer simulations presented in this paper were done at the National Center for Supercomputing Applications (NCSA) at Urbana-Champaign and at the National Energy Research Scientific Computing Center at the Lawrence Berkeley National Laboratory.

Sellwood J. A., 2002, private communication  
 Sellwood J. A., Athanassoula E., 1986, MNRAS, 221, 195  
 Tremaine S., Weinberg M. D., 1984, ApJ, 282, L5  
 van den Bosch F. C., Swaters R. A., 2001, MNRAS, 325, 1017  
 Weinberg M. D., 1985, MNRAS, 213, 451  
 Weinberg M. D., 1998, MNRAS, 297, 101  
 Weinberg M. D., Katz N., 2001, astro-ph, 1, 0110632  
 Zhao H., Mao S., 1996, MNRAS, 283, 1197  
 Zhao H. S., 1996, MNRAS, 283, 149

**REFERENCES**

Athanassoula E., Misiriotis A., 2002, MNRAS, 330, 35  
 Binney J. J., Evans N. W., 2001, MNRAS, 327, L27  
 Blitz L., Spiegel D. N., 1991, ApJ, 370, 205  
 Colín P., Klypin A. A., Kravtsov A. V., 2000, ApJ, 539, 561  
 Combes F., Sanders R. H., 1981, A&A, 96, 164  
 de Blok W. J. G., McGaugh S. S., Rubin V. C., 2001, AJ, 122, 2396  
 Debattista V. P., Sellwood J. A., 1998, ApJ, 493, L5  
 Debattista V. P., Sellwood J. A., 2000, ApJ, 543, 704  
 Dehnen W., Binney J., 1998, MNRAS, 294, 429  
 Eke V. R., Navarro J. F., Steinmetz M., 2001, ApJ, 554, 114  
 El-Zant A., Shlosman I., Hoffman Y., 2001, ApJ, 560, 636  
 Elmegreen B. G., Elmegreen D. M., 1985, ApJ, 288, 438  
 Flores R. A., Primack J. R., 1994, ApJ, 427, L1  
 Freudenreich H. T., 1998, ApJ, 492, 495  
 Fux R., 1997, Astronomy & Astrophysics, 327, 983  
 Gerhard O., 2002, astro-ph/0203109  
 Hammersley P. L., Cohen M., Garzón F., Mahoney T., López-Corredoira M., 1999, MNRAS, 308, 333  
 Hernández X., Avila-Reese V., Firmani C., 2001, MNRAS, 327, 329  
 Hernquist L., 1993, ApJS, 86, 389  
 Hernquist L., Weinberg M. D., 1992, ApJ, 400, 80  
 Hohl F., 1971, ApJ, 168, 343  
 Klypin A., Kravtsov A. V., Valenzuela O., Prada F., 1999, ApJ, 522, 82  
 Klypin A., Zhao H., Somerville R., 2002, ApJ, 573, xx  
 Knebe A., Kravtsov A. V., Gottlöber S., Klypin A. A., 2000, MNRAS, 317, 630  
 Kravtsov A. V., 1999, PhD  
 Kravtsov A. V., Klypin A. A., Bullock J. S., Primack J. R., 1998, ApJ, 502, 48  
 Kravtsov A. V., Klypin A. A., Khokhlov A. M., 1997, ApJS, 111, 73  
 Little B., Carlberg R. G., 1991, MNRAS, 251, 227  
 Lokas E. L., 2001, MNRAS, 327, L21  
 Miller R. H., 1978, ApJ, 224, 32  
 Moore B., 1994, Nature, 370, 629  
 Moore B., Ghigna S., Governato F., Lake G., Quinn T., Stadel J., Tozzi P., 1999, ApJ, 524, L19  
 Navarro J. F., Frenk C. S., White S. D. M., 1997, ApJ, 490, 493  
 Navarro J. F., Steinmetz M., 2000, ApJ, 528, 607  
 Ostriker J. P., Peebles P. J. E., 1973, ApJ, 186, 467